

Real-time monitoring of benzene, toluene, and *p*-xylene in a photoreaction chamber with a tunable mid-infrared laser and ultraviolet differential optical absorption spectroscopy

Matthew T. Parsons,^{1,*} Ihor Sydoryk,¹ Alan Lim,¹ Thomas J. McIntyre,¹ John Tulip,^{1,4} Wolfgang Jäger,^{2,5} and Karen McDonald³

¹Department of Electrical and Computer Engineering, University of Alberta,
9107 116 Street, Edmonton, Alberta, T6G 2V4, Canada

²Department of Chemistry, University of Alberta, 11227 Saskatchewan Drive, Edmonton,
Alberta, T6G 2G2, Canada

³Environmental Health, Concordia University College of Alberta, 7128 Ada Boulevard,
Edmonton, Alberta, T58 4E4, Canada

⁴E-mail: jtulip@telus.net

⁵E-mail: wolfgang.jaeger@ualberta.ca

*Corresponding author: mparsons@ualberta.ca

Received 28 June 2010; revised 9 December 2010; accepted 10 December 2010;
posted 14 December 2010 (Doc. ID 130685); published 26 January 2011

We describe the implementation of a mid-infrared laser-based trace gas sensor with a photoreaction chamber, used for reproducing chemical transformations of benzene, toluene, and *p*-xylene (BTX) gases that may occur in the atmosphere. The system performance was assessed in the presence of photoreaction products including aerosol particles. A mid-infrared external cavity quantum cascade laser (EC-QCL)—tunable from 9.41–9.88 μm (1012–1063 cm^{-1})—was used to monitor gas phase concentrations of BTX simultaneously and in real time during chemical processing of these compounds with hydroxyl radicals in a photoreaction chamber. Results are compared to concurrent measurements using ultraviolet differential optical absorption spectroscopy (UV DOAS). The EC-QCL based system provides quantitation limits of approximately 200, 200, and 600 parts in 10^9 (ppb) for benzene, toluene, and *p*-xylene, respectively, which represents a significant improvement over our previous work with this laser system. Correspondingly, we observe the best agreement between the EC-QCL measurements and the UV DOAS measurements with benzene, followed by toluene, then *p*-xylene. Although BTX gas-detection limits are not as low for the EC-QCL system as for UV DOAS, an unidentified by-product of the photoreactions was observed with the EC-QCL, but not with the UV DOAS system. © 2011 Optical Society of America

OCIS codes: 010.1030, 010.1120, 120.6200, 140.3600, 300.6340, 300.6540.

1. Introduction

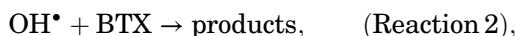
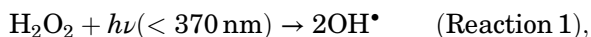
Air quality in both urban and rural environments is closely tied to the composition and chemical transfor-

mation of trace gas species in the atmosphere. A major challenge to improve air-quality prediction is to better understand the short-term chemical processes that affect secondary pollutant formation, including secondary organic aerosol formation [1]. Secondary organic pollutants, including aerosols, from trace gas precursor species are important when considering

0003-6935/11/040A90-10\$15.00/0
© 2011 Optical Society of America

air quality for their detrimental effects on environmental health and human health [2].

We focus our efforts on benzene, toluene, and xylene (BTX) gases, which are often associated with air emissions from petroleum production industries. Even without chemical transformation, these gases have multiple impacts on the environment and human health [2]. Benzene, for example, is listed as a toxic compound for its carcinogenic properties [2–4]. BTX gases have also been shown to form secondary pollutants in the troposphere, including compounds that can lead to photochemical smog and tropospheric ozone formation [5–7]. For the purposes of this study, we have chosen the well-known hydroxyl radical reaction pathway for chemical transformation of BTX gas species, generalized by



where products can react further and condense into secondary organic aerosol particles [8,9].

Regional air-quality monitoring programs are capable of measuring BTX gas concentrations in the atmosphere. These types of programs typically make use of air samples obtained over several days, with offline analysis of organic compounds using gas chromatography or mass spectrometry [10]. This strategy is useful for its ability to obtain spatially-resolved data over monitoring array networks, but it is labor intensive and lacks important real-time concentration information [11] that can be used to better characterize diurnal trends or accidental releases, for example.

Specialized studies are capable of monitoring BTX gases in the atmosphere using direct sampling to highly sensitive mass spectrometers, thus obtaining measurements in real time [11]. Fourier transform infrared (FTIR) spectroscopy has also been demonstrated to be a useful method for measurements of trace gases in the atmosphere [12–14]. However, these highly specialized, state-of-the-art instruments are more difficult to operate—due to physical constraints such as size, portability, vibration control, and electrical power requirements—and therefore unsuitable for implementation in local or regional continuous air-quality monitoring programs in networked arrays of instruments.

Differential optical absorption spectroscopy (DOAS) has been shown to be a useful method to detect numerous trace gases in the atmosphere [15–17], although this method is not commonly employed in regional air-quality monitoring networks. BTX gases are particularly well-suited for ultraviolet DOAS (UV DOAS) measurements due to the distinctive absorption properties of these gases in the range of 220–290 nm [15]. Despite the success of UV DOAS measurements, this measurement technique is limited by atmospheric attenuation of UV light, primar-

ily due to oxygen and ozone absorption, and is therefore restricted to path lengths of less than approximately 1 km [15,17].

Here we extend our previous trace gas measurements of benzene and toluene using a tunable quantum cascade laser in the mid-infrared (mid-IR) region [18]. This work describes significant improvements to this mid-IR laser system for BTX trace gas measurements. In this study, we measured concentrations of BTX trace gas species in real time with a tunable mid-IR laser absorption trace gas sensor, while these gases underwent photochemical reactions. The mid-IR laser is tunable between 9.41–9.88 μm (1012–1063 cm^{-1}), which is one of several atmospheric windows in the infrared region with minimal interference from water or CO_2 . Other atmospheric windows of interest for BTX gases include the 3–4 μm and 12–15 μm regions. We describe a photoreaction chamber used for reproducing chemical transformations of BTX gases that may occur in the atmosphere as a means to rate the performance of this spectroscopic method in the presence of photoreaction products including aerosol particles. Photoreaction chambers have frequently been used to study atmospheric processes such as these BTX reactions under well-controlled conditions (for example, see [6,8,19–21]). We compare our mid-IR measurements to concurrent UV spectroscopic concentration measurements of the same BTX trace gases, which is a well-established method to measure BTX gases [15–17]. To the best of our knowledge, mid-IR absorption spectroscopy with a tunable EC-QCL system has not been used to measure BTX gas concentrations in a photoreaction chamber.

As is the case for trace gas concentration measurements in the ambient atmosphere, these same measurements in photoreaction chambers often involve extractive gas chromatography or mass spectrometry [20–22]. A number of studies have successfully used *in situ* spectroscopic measurements in photoreaction chambers. For example, the European photoreactor (EUPHORE) can operate with *in situ* UV DOAS and FTIR spectroscopy [19].

We note that our intention with this work is not to compete with the high accuracy and resolution available to FTIR instruments, but rather to explore the viability of a tunable laser-based mid-IR spectroscopic method as a research tool for studying BTX gas processes and for practical applications in local and regional continuous, real-time air-quality monitoring programs.

2. Experimental

A schematic diagram of the experimental setup is shown in Fig. 1. Details of the major components of the experimental setup are described below.

A. Photoreaction Chamber

The photoreaction chamber used in this study is a cube constructed of 0.127 mm thick perfluoroalkoxy (PFA) film with a volume of 1.8 m^3 (Ingeniven

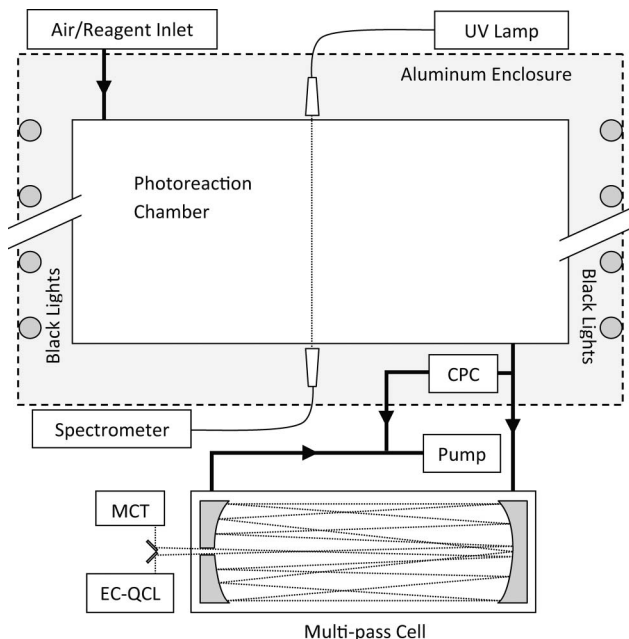


Fig. 1. Schematic diagram of experimental setup. Temperature was measured on the outer surfaces of the photoreaction chamber and outside the aluminum enclosure (dashed line). Temperatures were 25–30 °C within the aluminum enclosure and approximately 21 °C outside the aluminum enclosure. The condensation particle counter (CPC) was positioned inside the aluminum enclosure to operate at the same temperature as the photoreaction chamber. The UV deuterium lamp and spectrometer were positioned outside the aluminum chamber, with the UV light directed through optical fibres and collimating/collecting lenses. The optical paths are indicated with dotted lines and sample and gas flows are indicated with thick lines.

Fluoropolymer Solutions) supported in an aluminum enclosure. The chamber can be irradiated with UV light by an array of 24 fluorescent 32 W black lights with peak emission at 350 nm. A condensation particle counter (TSI, 3771) was installed at an outlet of the photoreaction chamber, inside the aluminum enclosure, to continuously monitor the total particle number density inside the photoreaction chamber. The particle counter can detect particles with diameters greater than 10 nm. Inlet and outlet tubing for the photoreaction chamber was made of PFA, conductive PFA, or stainless steel where appropriate (conductive silicone tubing was found to interfere with toluene sampling, and was therefore not used). All experiments were carried out with filtered, dry air diluting the contents of the photoreaction chamber while continuously sampling from the chamber to maintain a constant volume of the photoreaction chamber. Results are correspondingly corrected for dilution effects with $C'(t) = C(t)/\exp(-Q \cdot t/V)$, where $C'(t)$ is the dilution-corrected concentration of a component inside the photoreaction chamber at time t , $C(t)$ is the actual measured concentration of a component inside the photoreaction chamber at time t , Q is the volumetric flow rate of air entering and exiting the photoreaction chamber (approximately 3.5 L · min⁻¹ in these experiments), and V

is the volume of the photoreaction chamber (approximately 1800 L).

BTX gases [benzene (Caledon, 99%), toluene (Fisher Scientific, 99.9%), *p*-xylene (Fisher Scientific, 99.9%)] were introduced into the photoreaction chamber via flow of filtered, dry air over a liquid reservoir of benzene, toluene, or *p*-xylene. Reagent reservoirs were maintained at a temperature of approximately 21 °C for this study. BTX gases were allowed to diffuse within the sealed photoreaction chamber for at least 1 h. This timing prior to each experiment was found to result in adequate mixing of reagent gases, as demonstrated with stable concentrations determined by the spectroscopic methods described below. Once the BTX gases had mixed sufficiently, H₂O₂ was continuously supplied to the photoreaction chamber via flow of filtered, dry air over liquid H₂O₂ [Fisher Scientific, 30% (w/w) in water] reservoir for the duration of each experiment to maintain an excess of H₂O₂ inside the photoreaction chamber. After approximately 30 min of monitoring the BTX gas concentrations with H₂O₂ flowing into the photoreaction chamber, Reaction 1 was initiated by irradiating the chamber with the array of black lights. The time at which the array of black lights was turned on defines time $t = 0$. Thermocouples attached to the outside of the photoreaction chamber indicated temperatures between 25–30 °C during the reactions. Control experiments showed that secondary organic aerosol particle formation is dependent on both the presence of H₂O₂ and at least one BTX gas in the photoreaction chamber, and irradiation with the UV black lights.

Following each experiment, the photoreaction chamber was flushed with approximately 10 L · min⁻¹ of filtered, dry air and H₂O₂ gas while irradiated with the UV lights for at least 24 h, and then flushed without UV exposure using only filtered, dry air for at least 24 h. Our experiments showed that this method, which is similar to that of Murphy *et al.* [23], is sufficient to remove any detectable trace gases and residual particulate matter from the photoreaction chamber in preparation for the next experiment. In other words, background concentration of BTX gases in the photoreaction chamber prior to each experiment was less than 20, 40, and 10 parts in 10⁹ (ppb) for benzene, toluene, and *p*-xylene, respectively.

B. Mid-IR Tunable Laser System

The mid-IR system has been described in detail previously [18]. The light source for these measurements was a room temperature continuous wave external cavity quantum cascade laser (EC-QCL), tunable between 9.41–9.88 μm (1012–1063 cm⁻¹) with a resolution of 0.002 cm⁻¹ (Daylight Solutions, TLS-CW-MHF). The tunable range of the EC-QCL is useful in that it lies in one of several regions with minimal interference from common atmospheric species, including CO₂ and water. The wavelength of the EC-QCL is factory calibrated. Additional quality checks

were performed by measuring the wavelength of several discrete absorption lines in a pure CO₂ gas sample to ensure consistency in the wavelength calibration for the laser over time. No significant wavelength drifts in the EC-QCL output were observed during this study. Uncertainty in output wavelength and repeatability were found to be approximately 0.028 cm⁻¹ and 0.012 cm⁻¹, respectively, probably due to grating angle jitter between scans. The maximum laser output power is 40 mW and the laser beam divergence is <5 mrad. The maximum tuning rate of the laser was 5 cm⁻¹/s. In this study, 10 sequential mid-IR absorption spectra were averaged for each gas concentration measurement, taken at a rate of 2 scans/min. A two-stage thermoelectrically cooled photovoltaic IR detector was used for most measurements (Boston Electronics, PDI-2TE-10.6); for the remaining measurements, a liquid nitrogen cooled mercury-cadmium-telluride (MCT) photovoltaic IR detector (Kolmar Technologies, KMPV11) was used. All measurements were obtained at atmospheric pressure. The mid-IR detector signal-to-noise ratio was on the order of 60:1 in this study.

In all mid-IR experiments discussed here, an astigmatic Herriott multipass cell [24] was used with a total path length of approximately 70 m, mounted in an aluminum chamber with a volume of approximately 14.2 L with a ZnSe window. In most experiments, PFA tubing was used to flow sample gas and particles from the photoreaction chamber to the multipass cell; some duplicate experiments used conductive PFA tubing for sampling to the multipass cell. No filters were inserted between the photoreaction chamber and the multipass cell, *per se*. However, PFA tubing does not efficiently transport particles, and thus approximately 40% of the particles in the sample flow were eliminated through deposition in the tubing between the photoreaction chamber and the multipass cell, as determined with particle counter measurements. No particle loss was observed in the multipass cell itself or in conductive PFA tubing, also verified with particle counter measurements. We note that the presence of aerosol particles did not have any observable effect on the performance of the optics in the multipass cell, as verified with measurements of calibration gas standards before and after exposure to aerosol particles. Also, the presence of aerosol particles did not appear to influence the mid-IR gas concentration measurements. That is to say, gas concentrations were observed to agree within uncertainty limits when consecutive samples were taken through the PFA tubing (with approximately 60% particle transport efficiency) or through conductive PFA tubing (with approximately 100% particle transport efficiency).

All mid-IR absorption spectra were referenced to a sample of filtered, dry air measured at the start of each experiment. Sample gas was then flowed through the multipass cell at a rate of 2.0 L · min⁻¹ from the photoreaction chamber. Based on the volume of the multipass cell and the flow rate used,

trace gas concentrations in the multipass cell lagged behind the corresponding concentration in the photoreaction chamber by about 30 min and corrections to the data were made to account for this lag time. That is to say, $t - 30$ min is reported for all mid-IR data.

C. UV System

The light source for UV differential optical absorption spectroscopy measurements was a broadband deuterium lamp with emission output from 215–400 nm (Ocean Optics, D-2000-S). A grating-based UV spectrometer with a resolution of 0.118 nm was used for these measurements (Ocean Optics, HR-2000+). The UV spectrometer was factory calibrated. Additional quality checks were performed by measuring the wavelength of several discrete emission lines from the fluorescent black lights to ensure consistency in the wavelength calibration for the UV spectrometer over time. Wavelength drifts in the UV spectrometer were not observed in this study. An optical fiber and collimating lens was used to direct UV light from the deuterium lamp through the photoreaction chamber. Likewise, a collecting lens and optical fiber was used to direct UV light to the UV spectrometer. No windows were required since the PFA film is transparent to UV. The deuterium lamp and the UV spectrometer were positioned outside the aluminum enclosure of the photoreaction chamber and maintained at a temperature of approximately 21 °C.

UV experiments were made *in situ* with a single pass through the simulation chamber over a path length of 1.2 m. All UV absorption spectra were referenced to filtered, dry air at the start of each experiment. All UV results are based on averages of 5000 spectra, taken at a rate of 1500 spectra/min.

D. Differential Optical Absorption Spectroscopy

Differential optical absorption spectroscopy (DOAS) has been developed as a useful tool for measuring trace gases ([15,25], and references therein). The mid-IR and UV absorption spectra were transformed to differential optical absorption spectra using a method similar to that described in Plane and Saiz-Lopez [15]. Each absorption spectrum was fit to a ninth-order polynomial over the region of interest (240–286 nm for UV, and 9.61–9.80 μm for mid-IR). The polynomial fit was subtracted from the original absorption spectrum to remove broad features of the absorption spectrum and temporal drifts in the output power of the light source, resulting in a differential optical absorption spectrum that retains the sample gas absorption. The differential optical absorption spectra were fit with literature data of absorption cross-sections [26,27] using a least-squares fitting routine with iterations in gas concentrations to determine the observed concentration of each reagent gas. For our UV analyses, we used literature absorption cross-section data at 293 K with a resolution of 0.001 nm [27]; our mid-IR analyses used literature absorption cross-section data at 298 K with

a resolution of 0.06 cm^{-1} [26]. The literature data were interpolated to the same wavelength scale used by our instruments and then smoothed with a cubic spline fit during the fitting routine. Temperature effects were not accounted for in this analysis because small variations in temperature result in spectral fluctuations that are within the literature [26,27] and observed uncertainty limits for spectral data.

Observed gas concentrations from literature fitting results were converted to actual gas concentrations with a calibration method. Both the mid-IR and UV systems were calibrated for gas concentration measurements using a calibration gas generator (Kin-Tek 491-MB). The calibration gas generator provides a constant emission rate of a sample gas (i.e., one of benzene, toluene, or xylene) from a permeation tube at a preset temperature. The concentration of the sample gas can then be adjusted based on the flow rate of diluent gas between $0.1\text{--}5\text{ Std L} \cdot \text{min}^{-1}$. The emission rate from each permeation tube used in the calibration gas generator is calibrated and traceable to the National Institute of Standards and Technology (NIST). The mid-IR system was calibrated with calibration gas in the multipass sample cell. The UV system was calibrated with calibration gas in a separate single-pass sample cell (path length of 0.5 m , and volume of approximately 0.25 L). Calibration gas was not introduced into the photoreaction chamber to calibrate the UV system because the slow flow rates from the calibration gas generator would take an unreasonable amount of time (over 300 h in some cases) to fill the volume of the photoreaction chamber. The resulting calibration curve is shown in Fig. 2 with conversion factors of $1\text{ }\mu\text{g m}^{-3} = X\text{ ppb}$ where $X = 3.17, 3.74,$ and 4.31 for benzene, toluene, and xylene, respectively, for our experimental conditions.

For the mid-IR measurements described here, indeed, with any extractive measurement, there are

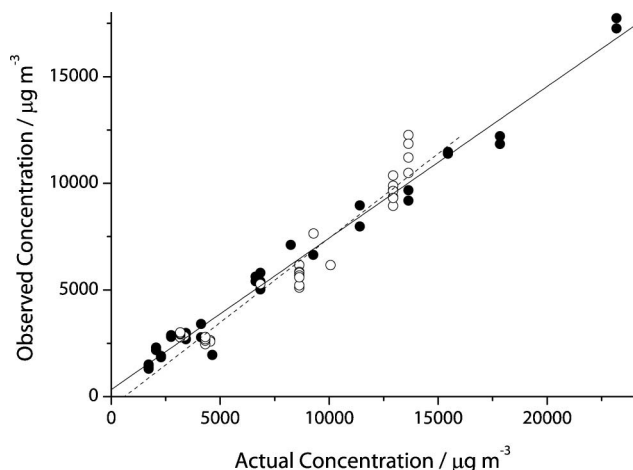


Fig. 2. Combined gas concentration calibration data for benzene, toluene, and xylene gases. Mid-IR data are shown as open symbols, with the dashed curve indicating the best linear fit through the data. UV data are shown as filled symbols, with the solid curve indicating the best linear fit through the data.

possible systematic errors, interferences, losses, and uncertainties associated with the sampling process itself (e.g., adsorption/desorption of gases on multipass cell or tubing walls). Our use of gas concentration calibrations described above was a major part of our solution to overcome many of these issues associated with extractive measurements. We have also characterized our instruments under various conditions including different dimensions and materials for sample flow tubing, different sequences of calibration gases, and measurements while diluting and filling calibration gases to have a thorough understanding of the interactions of the gases with our equipment and confidence in our results.

We also performed separate static experiments during this study (i.e., the photoreaction chamber without black light irradiation and the mid-IR multipass cell were both sealed for several hours) to confirm that measured gas concentrations were not significantly affected by wall adsorption over time, at least within the uncertainty of the measurements.

3. Results and Discussion

Results are shown for spectroscopic measurements of BTX gas species in the mid-IR and UV ranges. These results illustrate the ability to monitor concentrations of multiple BTX gas species in real time using these methods during chemical transformation processes in a photoreaction chamber.

Figures 3 and 4 show typical examples of mid-IR and UV differential optical absorption spectra, respectively, of mixed benzene + *p*-xylene and mixed benzene + toluene + *p*-xylene contained in the photoreaction chamber prior to initiating the reaction inside the photoreaction chamber. Also shown

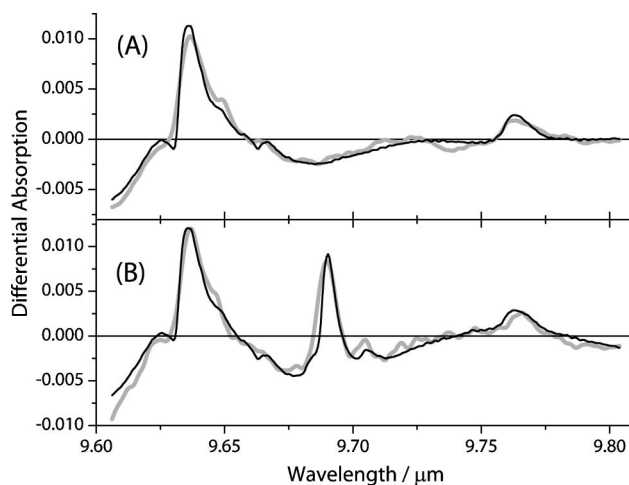


Fig. 3. Mid-IR differential optical absorption spectra of (A) benzene (3.8 ppm) + *p*-xylene (3.6 ppm), and (B) benzene (3.9 ppm) + toluene (4.6 ppm) + *p*-xylene (3.0 ppm). The path length for these measurements was approximately 70 m . Benzene, toluene, and *p*-xylene absorb at approximately $9.63\text{ }\mu\text{m}$, $9.69\text{ }\mu\text{m}$, and $9.77\text{ }\mu\text{m}$, respectively. The thick gray curves are observed data and the thin black curves are fits to literature data [26]. Literature spectra have an uncertainty of 3%, and the observed spectra have an uncertainty of 6%.

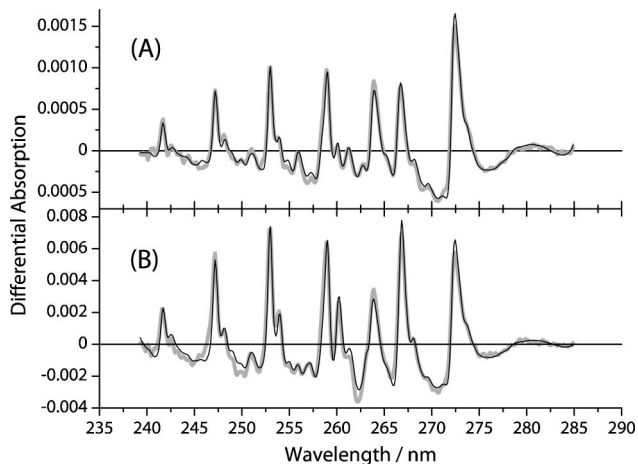


Fig. 4. UV differential optical absorption spectra of (A) benzene (1.1 ppm) + *p*-xylene (1.2 ppm), and (B) benzene (3.9 ppm) + toluene (4.6 ppm) + *p*-xylene (2.1 ppm). The path length for these measurements was 1.2 m. Although each component has several overlapping absorption features in this region, benzene, toluene, and *p*-xylene have peak absorption at approximately 253 nm, 267 nm, and 272 nm, respectively. The relative heights of absorption features are critical to determine component gas concentrations. The thick gray curves are observed data and the thin black curves are fits to literature data [27]. Literature and observed spectra have an uncertainty of approximately 1%.

in Figs. 3 and 4 are the corresponding best fits from literature data [26,27] used to obtain the concentrations of benzene, toluene, and *p*-xylene in the sample gas noted in the figure captions. The observed spectra for these mixtures shown in Figs. 3 and 4 are in good agreement with the corresponding literature spectra. These results emphasize the ability to monitor multiple BTX gas species simultaneously with either a UV spectrometer, or a mid-IR tunable EC-QCL based spectrometer.

We calculated the detection limits and limits of quantitation for each BTX gas measured with the mid-IR and UV systems based on our current path lengths. The detection limits are based on the value of $3s_i/m$, where s_i is the standard deviation of the observed background concentration of gas i in a blank sample, and m is the slope of the calibration curve for all gases [28]. Similarly, we calculated the limits of

quantitation for each BTX gas measured with the mid-IR and UV systems based on the value of $10s_i/m$ [28]. Results of this analysis are outlined in Table 1. Detection and quantitation limits for the mid-IR differential optical absorption measurements show considerable improvement from our previous study [18], likely as a result of laser stability improvements, from replacing the laser head to include a higher quality antireflection coating on the laser diode, and through using the DOAS fitting routine to obtain gas concentrations. The UV system shows lower limits of detection and quantitation than those of the mid-IR system. This is due to the fact that BTX gases have several distinct features in the absorption spectra in the range of the UV measurements, as opposed to single peaks and broad features in the absorption spectra in the range of the mid-IR measurements. DOAS in any wavelength region performs best when the molecules of interest have multiple absorption features rather than a strong absolute absorption [15].

The uncertainty in measurements of BTX gas concentration for the mid-IR and UV systems was calculated based on twice the uncertainty derived from the linear regression results of the calibration curves [29]. We doubled this calculated uncertainty to maintain a conservative estimate of the uncertainty in all of our results and to better represent the observed repeatability in the calibration data. Uncertainty limits for the mid-IR and UV measurements are also listed in Table 1. Generally, uncertainty is less than or equal to the corresponding limit of quantitation for each gas for mid-IR and UV measurements with the exception of *p*-xylene with UV, where the difference is a result of rounding to a single significant figure.

Figure 5 shows an example of mid-IR and UV DOAS data obtained during chemical transformation of a mixture of benzene + *p*-xylene with hydroxyl radicals in the photoreaction chamber as a function of time. The initial concentration of benzene was 3.8 ppm and the initial concentration of *p*-xylene was 2.5 ppm. Likewise, Fig. 6 shows an example of these measurements during chemical transformation of a mixture of benzene + toluene + *p*-xylene with hydroxyl radicals with initial concentrations of 3.7, 4.8, and 2.0 ppm for

Table 1. Specifications and Performance Comparison between Mid-IR and UV Systems

Compound	Mid-IR			UV		
	Detection Limit (ppb)	Limit of Quantitation (ppb)	Uncertainty (ppb)	Detection Limit (ppb)	Limit of Quantitation (ppb)	Uncertainty (ppb)
Benzene	60	200	200	20	70	60
Toluene	70	200	200	40	100	50
<i>p</i> -Xylene	200	600	200	10	30	40
Path Length (m)	70			1.2		
Full Wavelength Range	9.41–9.88 μm (1012–1063 cm^{-1})			215–400 nm		
Resolution	0.002 cm^{-1}			0.118 nm		
Scans Averaged	10			5000		
Scan Rate (min^{-1})	2			1500		

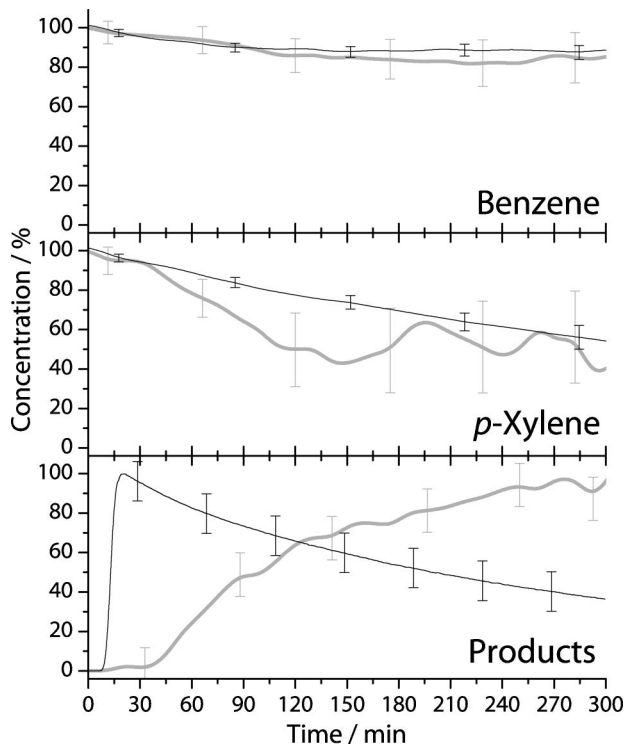


Fig. 5. Benzene and *p*-xylene gas concentration measurements in the photoreaction chamber as a function of time. Mid-IR data are shown as thick gray curves and UV data are shown as thin black curves. The products panel shows normalized secondary organic aerosol particle number density as a thin black curve and normalized by-product concentration as a thick gray curve. All data were corrected to account for dilution of the photoreaction chamber content over the course of the reaction, as described in the text.

benzene, toluene, and *p*-xylene, respectively. These data are representative of duplicate experiments—each experiment was duplicated at least twice—and results were consistently within the uncertainty limits shown here. Figures 5 and 6 show the measured gas concentrations as a percentage of the original concentration of each gas after corrections for dilution of the photoreaction chamber content. Dilution corrections become more substantial with increasing time as the actual concentrations of reagent gases approach detection limits outlined in Table 1. This is reflected with the increasing magnitude of error bars in Figs. 5 and 6. There is good agreement between measurements of benzene concentration from the mid-IR and UV systems shown in Figs. 5 and 6. For the toluene data shown in Fig. 6, some minor deviations between the mid-IR and UV systems are seen after the first hour of the reaction. It is possible that this may be a result of toluene depositing on the walls of the mid-IR multipass cell and slowly desorbing. This would be consistent with our observation that it was difficult to sample toluene through conductive silicone tubing due to depletion along the tubing walls. Meanwhile, *p*-xylene concentration measurements do not show good agreement between mid-IR and UV systems. Although the qualitative trend is similar in both mid-IR and UV data sets for *p*-xylene shown in Fig. 5,

there is considerable fluctuation in the *p*-xylene concentration data from the mid-IR system. In Fig. 6, UV data show a steady reduction in *p*-xylene concentration, whereas the mid-IR data show no significant change over the time period of the experiment. As noted above, the DOAS method performs best when molecules of interest show numerous absorption peaks in the wavelength range used [15]. In the mid-IR range of the EC-QCL, *p*-xylene exhibits only a single small absorption peak, which results in a higher quantitation limit compared to benzene and toluene and thus concentration measurements of *p*-xylene gas from this method become difficult as the reaction proceeds and *p*-xylene concentration approaches the detection limit.

The combined data in Figs. 5 and 6 also show that over the time scale of these reactions, the concentration of benzene is observed to change at a smaller

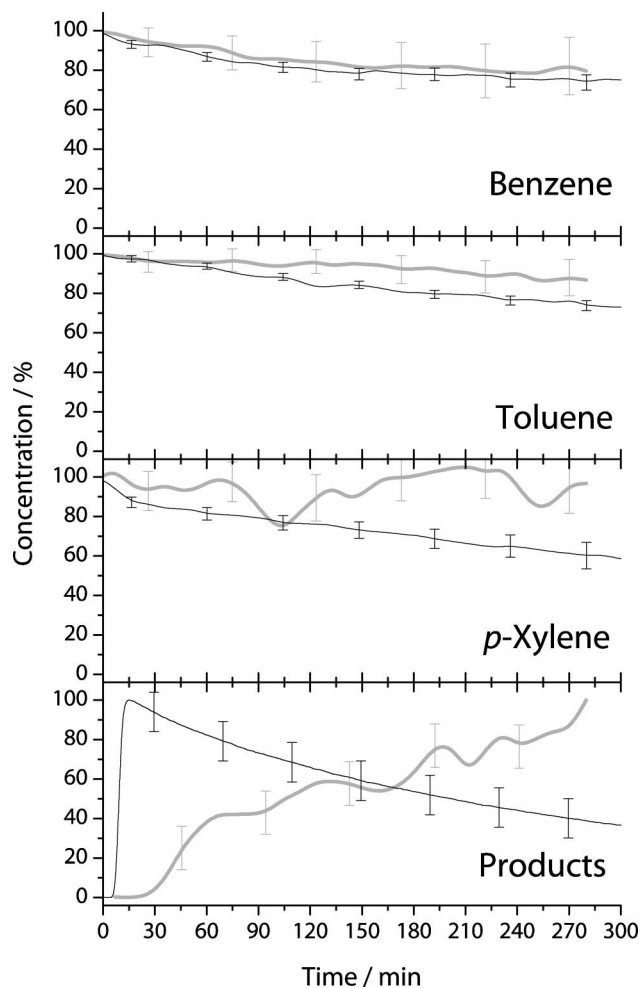


Fig. 6. Benzene, toluene, and *p*-xylene gas concentration measurements in the photoreaction chamber as a function of time. Mid-IR data are shown as thick gray curves, UV data are shown as thin black curves. The product panel shows normalized secondary organic aerosol particle number density as a thin black curve and normalized by-product concentration as a thick gray curve. All data were corrected to account for dilution of the photoreaction chamber content over the course of the reaction, as described in the text.

rate than that of toluene, which in turn is observed to change at a smaller rate than that of *p*-xylene. This observed ranking of reactivity is consistent with the published rates of reaction for benzene, toluene, and *p*-xylene with hydroxyl radicals according to Reaction 2 (1.22 , 5.63 , and $14.3 \times 10^{-12} \text{ cm}^3 \cdot \text{molecule}^{-1} \cdot \text{s}^{-1}$, for benzene, toluene, and *p*-xylene, respectively [9]).

The reactions of benzene + *p*-xylene and benzene + toluene + *p*-xylene with hydroxyl radicals resulted in significant secondary organic aerosol particle formation with the reagent gas concentrations used here, as indicated by the particle number density data represented in Figs. 5 and 6. This is consistent with previous studies showing that BTX gases are precursors for secondary organic aerosol particle formation [6,7]. In these figures, we have plotted the corresponding normalized particle number density in the photoreaction chamber after a correction for dilution of the photoreaction chamber content. In the cases shown here, particles were observed to reach a maximum number density of approximately $55,000 \text{ cm}^{-3}$. Note that the aerosol particle formation process is not immediate, but rather there is an accumulation period during which the concentrations of product gases increase prior to particle nucleation. This behavior is typical of aerosol chamber studies that do not use seed particles (for example, see Song *et al.* [22]). Furthermore, particle number density reaches a maximum and eventually decreases in these figures, which is associated with particle coagulation, settling, and other loss processes. Spectral signatures of particles were not clearly observed in either mid-IR or UV data.

In addition to secondary organic aerosol particle formation, we also observed formation of a by-product in the reactions of hydroxyl radicals with benzene + *p*-xylene and with benzene + toluene + *p*-xylene. Figure 7 shows an example of mid-IR DOAS spectra for both benzene + *p*-xylene and benzene + toluene + *p*-xylene reactions at 0, 1, and 5 hours of the reactions (without dilution corrections). This figure shows that, as the reaction proceeds, the intensities of the differential absorption peaks for benzene, toluene, and *p*-xylene gases are observed to decrease, thus indicating a decrease in concentration of these gases (as indicated in Figs. 5 and 6). Meanwhile, an absorption feature at approximately $9.67 \mu\text{m}$ is observed to increase in intensity beyond the noise observed in the spectra as the reactions proceed. Glyoxal, methylglyoxal, 3-hexene-2,5-dione, 2,5-dimethylphenol, and 3-methyl-2,5-furandione are among the most abundant organic products from the photoreactions in this study [30,31]. Available mid-IR spectra for these and other (H_2O_2 , H_2O , O_3) compounds do not show any agreement with the observed spectra. An unambiguous identification of the molecular carrier of this spectral feature will require extensive kinetic modeling studies. Thus, we simply label this feature as that of a by-product of the reactions without speculations

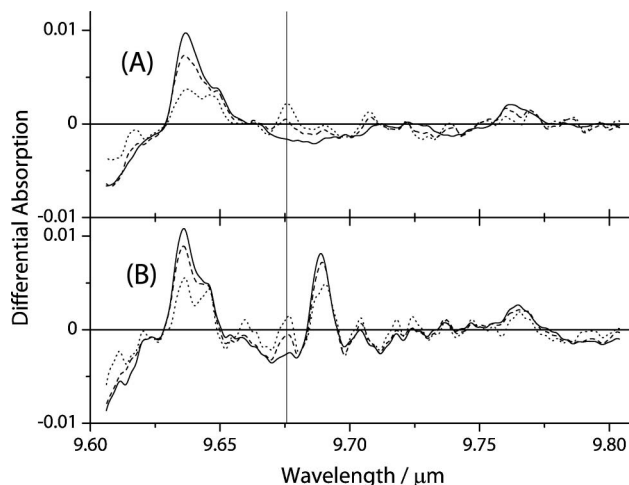


Fig. 7. Mid-IR differential optical absorption spectra at specific time intervals for (A) benzene + *p*-xylene, and (B) benzene + toluene + *p*-xylene. Solid spectra are at $t = 0$ h, dashed spectra are at $t = 1$ h (without dilution correction), and dotted spectra are at $t = 5$ h (without dilution correction). Benzene, toluene, and *p*-xylene absorb at approximately $9.63 \mu\text{m}$, $9.69 \mu\text{m}$, and $9.77 \mu\text{m}$, respectively. A reaction by-product peak is observed in both cases at $9.67 \mu\text{m}$, as indicated by the vertical line through the spectra. Uncertainty in observed spectra is 6%.

to identify the compound(s) responsible for this observation.

No corresponding absorption features from by-products were observed in the UV DOAS spectra during these experiments, either in the BTX spectral window (240–286 nm), or in the full range of the UV spectrometer (215–400 nm). It is possible that the by-product has UV absorption outside the range of the UV spectrometer, or that the by-product has only very broad absorption features that are not visible in differential absorption spectra in the range of the UV spectrometer. For example, glyoxal has UV absorption primarily $>400 \text{ nm}$ with only very broad UV absorption $<400 \text{ nm}$ [32].

We also show the by-product concentration profile as a function of time in Figs. 5 and 6. Here we calculated the area of the by-product absorption feature in the mid-IR differential absorption spectra between 9.66 – $9.68 \mu\text{m}$, made appropriate dilution corrections as described above, and normalized the resulting profile to span from 0% at $t = 0$ min to 100% at the maximum observed concentration. The resulting concentration profile for the by-product appears to exhibit logarithmic growth, possibly towards a steady-state condition where the rate of by-product formation approaches the rate of by-product loss, presumably through subsequent reactions with compounds in the photoreaction chamber.

4. Conclusions

We have demonstrated the use of a mid-IR tunable EC-QCL based spectrometer to monitor BTX trace gas concentration in real time during chemical transformation processes in a photoreaction chamber. The results are compared to concurrent measurements of

these gases with a UV DOAS system. We found good agreement between the mid-IR and UV systems for benzene concentration measurements, but only limited agreement between the mid-IR and UV systems for toluene, possibly due to adsorption of toluene on the mid-IR multipass cell. For *p*-xylene, we observed poor agreement between the mid-IR and UV systems since this compound does not have strong absorption in the wavelength range of the EC-QCL source.

Our current mid-IR measurements are based on continuous sampling of gas from a photoreaction chamber into a multipass cell. The UV measurements were made *in situ*, with a single-pass optical path directly through the photoreaction chamber. The mid-IR system is particularly well-suited for longer, open-path measurements because it uses a laser light source with minimal beam divergence in a region with minimal interference from absorption of atmospheric components, including carbon dioxide and water. Furthermore, particles were found not to degrade the IR system performance. In contrast, the UV source used in this study has significant beam divergence for path lengths greater than 4 m, and UV light suffers from significant oxygen and ozone absorption and particle scattering at longer path lengths in this wavelength region.

Our results show the formation of secondary species including particulate matter and a by-product from reactions of BTX gases with hydroxyl radicals. We stress that the by-product from these reactions was only observed in the mid-IR measurements, illustrating the usefulness of this particular wavelength range in studying BTX gas reactions both in photoreaction chambers and in the ambient atmosphere. This study demonstrates that this type of mid-IR system has the potential to be beneficial as a research tool for trace gas analysis and as a component of local or regional continuous atmospheric trace gas monitoring programs due to its minimal size, vibration control, and electrical power requirements.

This work was supported by the Natural Sciences and Engineering Research Council of Canada, the National Research Council of Canada (NRC), and the Development Bank of Canada.

References

1. G. R. Carmichael, A. Sandu, T. Chai, D. N. Daescu, E. M. Constantinescu, and Y. Tang, "Predicting air quality: Improvements through advanced methods to integrate models and measurements," *J. Comput. Phys.* **227**, 3540–3571 (2008).
2. M. Lippmann, *Environmental Toxicants: Human Exposures and Their Health Effects* (Wiley, 2009).
3. "Interaction Profile for: Benzene, Toluene, Ethylbenzene, and Xylenes (BTEX)," (Agency for Toxic Substances and Disease Registry, 2004).
4. J. Whysner, M. V. Reddy, P. M. Ross, M. Mohan, and E. A. Lax, "Genotoxicity of benzene and its metabolites," *Mutat. Res.* **566**, 99–130 (2004).
5. J. H. Seinfeld and S. N. Pandis, *Atmospheric Chemistry and Physics: From Air Pollution to Climate Change* (Wiley, 2006).
6. N. L. Ng, J. H. Kroll, A. W. H. Chan, P. S. Chhabra, R. C. Flagan, and J. H. Seinfeld, "Secondary organic aerosol formation from *m*-xylene, toluene, and benzene," *Atmos. Chem. Phys.* **7**, 3909–3922 (2007).
7. M. Martín-Reviejo and K. Wirtz, "Is benzene a precursor for secondary organic aerosol?," *Environ. Sci. Technol.* **39**, 1045–1054 (2005).
8. B. J. Finlayson-Pitts and J. N. Pitts, *Chemistry of the Upper and Lower Atmosphere: Theory, Experiments and Applications* (Academic, 2000).
9. J. G. Calvert, R. Atkinson, K. H. Becker, R. M. Kamens, J. H. Seinfeld, T. J. Wallington, and G. Yarwood, *The Mechanisms of Atmospheric Oxidation of Aromatic Hydrocarbons* (Oxford University Press, 2002).
10. H. Skov, A. Lindskog, F. Palmgren, and C. S. Christensen, "An overview of commonly used methods for measuring benzene in ambient air," *Atmos. Environ.* **35**, S141–S148 (2001).
11. K. Badjagbo, S. Moore, and S. Sauve, "Real-time continuous monitoring methods for airborne VOCs," *Trends Anal. Chem.* **26**, 931–940 (2007).
12. Z. Bacsik, J. Mink, and G. Keresztury, "FTIR spectroscopy of the atmosphere Part 2. Applications," *Appl. Spectrosc. Rev.* **40**, 327–390 (2005).
13. R. J. Yokelson, R. Susott, D. E. Ward, J. Reardon, and D. W. T. Griffith, "Emissions from smoldering combustion of biomass measured by open-path Fourier transform infrared spectroscopy," *J. Geophys. Res.* **102**, 18865–18877 (1997).
14. H. M. Heise, U. Muller, A. G. Gartner, and N. Holscher, "Improved chemometric strategies for quantitative FTIR spectral analysis and applications in atmospheric open-path monitoring," *Field Anal. Chem. Technol.* **5**, 13–28 (2001).
15. J. M. C. Plane and A. Saiz-Lopez, "UV-visible differential optical absorption spectroscopy," in *Analytical Techniques for Atmospheric Measurement*, D. E. Heard, ed. (Blackwell, 2006), pp. 147–188.
16. R. Volkamer, L. T. Molina, M. J. Molina, T. Shirley, and W. H. Brune, "DOAS measurement of glyoxal as an indicator for fast VOC chemistry in urban air," *Geophys. Res. Lett.* **32**, L08806 (2005).
17. R. Volkamer, T. Etzkorn, A. Geyer, and U. Platt, "Correction of the oxygen interference with UV spectroscopic (DOAS) measurements of monocyclic aromatic hydrocarbons in the atmosphere," *Atmos. Environ.* **32**, 3731–3747 (1998).
18. I. Sydoryk, A. Lim, W. Jäger, J. Tulip, and M. T. Parsons, "Detection of benzene and toluene gases using a midinfrared continuous-wave external cavity quantum cascade laser at atmospheric pressure," *Appl. Opt.* **49**, 945–949 (2010).
19. B. Klotz, S. Sorensen, I. Barnes, K. H. Becker, T. Etzkorn, R. Volkamer, U. Platt, K. Wirtz, and M. Martín-Reviejo, "Atmospheric oxidation of toluene in a large-volume outdoor photoreactor: In situ determination of ring-retaining product yields," *J. Phys. Chem. A* **102**, 10289–10299 (1998).
20. H. Takekawa, H. Minoura, and S. Yamazaki, "Temperature dependence of secondary organic aerosol formation by photo-oxidation of hydrocarbons," *Atmos. Environ.* **37**, 3413–3424 (2003).
21. W. P. L. Carter, D. R. Cocker, D. R. Fitz, I. L. Malkina, K. Bumiller, C. G. Sauer, J. T. Pisano, C. Bufalino, and C. Song, "A new environmental chamber for evaluation of gas-phase chemical mechanisms and secondary aerosol formation," *Atmos. Environ.* **39**, 7768–7788 (2005).
22. C. Song, K. Na, B. Warren, Q. Malloy, and D. R. Cocker, "Secondary organic aerosol formation from *m*-xylene in the absence of NO_x," *Environ. Sci. Technol.* **41**, 7409–7416 (2007).
23. S. M. Murphy, A. Sorooshian, J. H. Kroll, N. L. Ng, P. Chhabra, C. Tong, J. D. Surratt, E. Knipping, R. C. Flagan, and J. H. Seinfeld, "Secondary aerosol formation from atmospheric

- reactions of aliphatic amines," *Atmos. Chem. Phys.* **7**, 2313–2337 (2007).
24. J. B. McManus, P. L. Keabian, and W. S. Zahniser, "Astigmatic mirror multipass absorption cells for long-path-length spectroscopy," *Appl. Opt.* **34**, 3336–3348 (1995).
 25. U. Platt, "Differential Optical Absorption Spectroscopy (DOAS)," in *Air Monitoring by Spectroscopy Techniques*, M. W. Sigrist, ed. (Wiley, 1994), pp. 27–83.
 26. S. W. Sharpe, T. J. Johnson, R. L. Sams, P. M. Chu, G. C. Rhoderick, and P. A. Johnson, "Gas-phase databases for quantitative infrared spectroscopy," *Appl. Spectrosc.* **58**, 1452–1461 (2004).
 27. S. Fally, M. Carleer, and A. C. Vandaele, "UV Fourier transform absorption cross sections of benzene, toluene, meta-, ortho-, and para-xylene," *J. Quant. Spectrosc. Radiat. Transfer* **110**, 766–782 (2009).
 28. D. A. Skoog, F. J. Holler, and T. A. Nieman, *Principles of Instrumental Analysis* (Brooks/Cole: Thomson Learning, 1998).
 29. D. C. Harris, *Quantitative Chemical Analysis* (W. H. Freeman, New York, 1999).
 30. H. J. L. Forstner, R. C. Flagan, and J. H. Seinfeld, "Secondary organic aerosol from the photooxidation of aromatic hydrocarbons: Molecular composition," *Environ. Sci. Technol.* **31**, 1345–1358 (1997).
 31. D. F. Smith, T. E. Kleindienst, and C. D. McIver, "Primary product distributions from the reaction of OH with *m*-, *p*-xylene, 1,2,4- and 1,3,5-trimethylbenzene," *J. Atmos. Chem.* **34**, 339–364 (1999).
 32. R. Volkamer, P. Spietz, J. Burrows, and U. Platt, "High-resolution absorption cross-section of glyoxal in the UV-vis and IR spectral ranges," *J. Photochem. Photobiol., A* **172**, 35–46 (2005).